Measurement of Flame Propagation Through Step Changes in Mixture Composition

by

Caroline Sorensen

Submitted to the Department of Mechanical Engineering
in partial fulfillment of the requirements for the degree of

Master of Science in Mechanical Engineering

at the

MASSACHUSETTS INSTITUTE OF TECHNOLOGY

June 2016

Signature redacted

Author .....
Department of Mechanical Engineering
May 23, 2016

Signature redacted

Certified by .....
Wai K. Cheng, Professor of Mechanical Engineering
Director, Sloan Automotive Laboratory
Thesis Supervisor

Signature redacted

Accepted by .....
Rohan Abeyaratne, Professor of Mechanical Engineering
Chairman, Department Committee on Graduate Students

Measurement of Flame Propagation Through Step Changes in Mixture Composition

by

Caroline Sorensen

Submitted to the Department of Mechanical Engineering
on May 23, 2016, in partial fulfillment of the
requirements for the degree of
Master of Science in Mechanical Engineering

Abstract

Flame speed is a central metric in the field of combustion. While particular mixtures have characteristic flame speeds, it has also been shown that in compositionally stratified mixtures, flames exhibit a path dependency, or memory effect. The goal of the experimental work presented in this thesis was to investigate the behavior of flame speed over step changes in equivalence ratios. This sharp stratification was achieved using a soap bubble blown at the center of a combustion bomb. A laser was used to ignite the mixture from the center. Flame speed was calculated from both a pressure trace analysis and from measuring the movement of the flame front through high speed Schlieren imaging. Both methods demonstrated good correlation with the literature for homogeneous charges. However, the analysis necessarily assumes a spherical flame, but the Schlieren video showed that the laser ignition system induced a significant protrusion in the flame front. This protrusion smooths the transition from the flame speed of the inner mixture to that of the outer. Therefore, it was demonstrated that this setup is not suitable for the measurement of flame speed transitional behavior over step-changes in equivalence ratio.

Thesis Supervisor: Wai K. Cheng, Professor of Mechanical Engineering
Title: Director, Sloan Automotive Laboratory

Nomenclature

κ	flame stretch rate	m	mass
$\mathbb{R}$	universal gas constant	MW	molecular weight
$\mathcal{D}$	mass diffusivity	P	pressure
$\mathscr{L}$	Markstein length	r	radius
ϕ	equivalence ratio	S_L	flame speed
ρ	density	T	temperature
A_f	area of flame front	t	time
c_p	specific heat at constant pressure	V	volume
L	diffusion mixing layer thickness	x	mass fraction

Contents

List of Figures

Chapter 1

Introduction

Flame speed is an essential metric in characterizing combustion. While several parameters determine the characteristic flame speed of a particular mixture (composition, temperature, pressure, etc), decades of work in the field have rendered flame speed a well-defined quantity in many situations [1–3].

The flame speed of the fuel-air charge in an internal combustion engine contributes to controllability, emissions, and efficiency. However, not all engines use fully homogeneous mixtures. The flame propagation through mixtures with stratified composition is a field of interest for engine designers looking to increase performance with fuel stratification strategies. Flames moving through stratified charges exhibit behavior different from that which would be expected from the local composition. This means that a flame's history, or memory, partially determines its behavior. The upstream equivalence ratio can raise or lower the local flame speed, and can even extend the limits of flammability in both the rich and lean extremes [4, 5].

Researchers have approached this phenomenon from many directions. Several studies have investigated particular engines and how they react to changes in fuel stratification [6,7]. Other have examined the more fundamental question through numerical [8–10] and experimental studies [11]. There are many parameters to consider: the fuel in question, the stoichiometry gradient, the presence of turbulence [12].

One of the earliest studies on this topic was done at the MIT Sloan Lab by Youngchul Ra [13]. His thesis presented evidence of the flame memory effect as seen

in flames propagating through step changes in equivalence ratio. While such step-changes are rare in practical applications, they can illuminate the underlying physics in the combustion process. The original motivation of this study was to extend his finding into other fuels and initial pressures. In order to achieve a step-stratified mixture, a soap bubble was used to separate two mixtures of different composition within a combustion bomb.

In experimental studies, the flame speed is generally measured either via the pressure record of the combustion vessel, or via visual record of the flame propagation. The pressure record obliges the researcher to make assumptions about the flame geometry [13], while the video analysis method requires knowledge of the velocity field around the flame front (either by assuming a simple geometry or by using particle image velocimetry) [11]. This work uses both methods to measure flame speed in a spherical combustion bomb.

Flame speed experiments often use spark plugs or lasers to ignite the mixtures. The experiments presented in this thesis used a laser in order to ignite the mixture at the center of the bubble inside the combustion sphere. High speed Schlieren imaging [14] of the experiments showed a major deviation from one of the central assumptions of both this work and that of Ra [13]. Namely, the laser ignition process caused a non-spherical flame front. The laser energy deposition created a repeatable lobe protruding from the otherwise spherical flame front, as documented is several other studies [15–17]. This phenomenon prevented the precise determination of the flame speed over the interface between two compositionally varied mixtures. The specifics of this finding are detailed in the following chapters.

Chapter 2

Methodology

This chapter describes the methodology used for this study. The chapter is divided into two main sections: one describes the physical experimental setup and the other presents the data analysis.

2.1 Experimental Setup

The goal of the experiment was to measure how flame speed changes as it crosses a sharp boundary in equivalence ratio. The equivalence ratio, ϕ, defined by equation 2.1, is the ratio of the mass of fuel to the mass of air, divided by the stoichiometric fuel-air ratio.

$$\phi = \frac{\frac{m_f}{m_a}}{(\frac{m_f}{m_a})_{stoich}} \tag{2.1}$$

Creating a step change in equivalence ratio is a two-step process: first, the combustion bomb was filled with a fuel-air mixture of a certain equivalence ratio, which is referred to as mixture 2. Then we use a different equivalence ratio mixture (mixture 1) to blow a soap bubble inside the combustion chamber. The bubble was centered inside the bomb, and a laser ignited the mixture at the center of the bubble. Ideally, this produces a spherical flame front which propagates outwards through the inner mixture until the flame reaches the interface of the two mixtures and instantly crosses

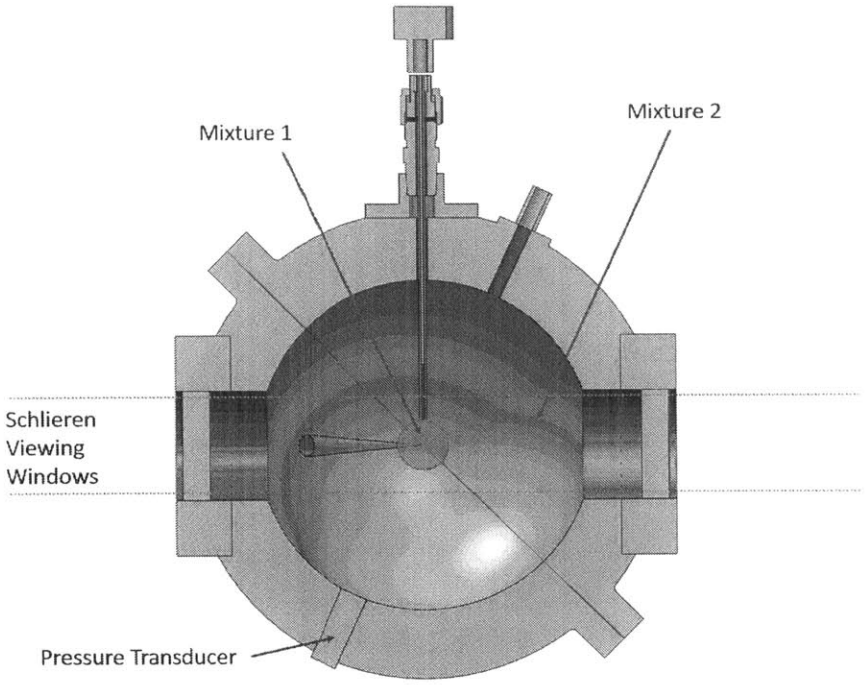

Figure 2-1: This schematic of combustion bomb setup shows the straw extending down from the top of the spherical combustion chamber. The bubble of mixture 1 is blown through this straw and ignited at its center by the focused laser beam shown in green. Quartz windows on either side provide direct viewing for the Schlieren system.

into the outer mixture with a different equivalence ratio (mixture 2). The setup is shown in figure 2-1.

The desire for a spherical flame front motivated the use of a laser to ignite the mixture at the center of the bomb. A frequency-doubled, neodymium-doped yttrium aluminum garnet laser provides a 4-6 ns pulse of approximately 160 mJ of energy at 532 nm wavelength. This laser pulse was directed through a focusing lens embedded in the wall of the bomb by a series of mirrors that filter out traces of unwanted wavelengths. Directly in front of the embedded wall lens was a pair of lenses - one plano-convex and the other bi-concave. By slightly changing the spacing between this pair of lenses, it was possible to marginally adjust the laser's focus point along the beam's axis. The embedded lens focused the beam to a small enough spot at the center of the bomb such that the energy was concentrated enough to create

ignition. Further discussion of the imperfections of the ignition system are discussed in subsection 3.1.2.

The soap bubble method allowed for total separation of the two different mixtures up until the instant of ignition (at which point the bubble bursts). The two mixtures were prepared in separate mixing tanks. By first metering into each evacuated tank the small amount of fuel required, and then filling the tanks with dry air, mixtures within 1-2 % of the desired equivalence ratio were achieved. The bomb was evacuated to less than 0.1 psia between combustion tests to preserve this tolerance level in the equivalence ratio. The bomb had two ports for filling and evacuating. One was controlled by a ball valve, while the other fitted a removable straw through which the bubble was blown. The straw had an 3.18 mm outer diameter and extended $\sim$ 64mm from the top of the inside surface of the bomb. The tip of the straw had a $\sim$ 0.15mm diameter hole for slow, controlled bubble blowing. The soap bubble had negligible effect on the combustion of the contents of the bomb. This is demonstrated by the nearly indistinguishable pressure traces between two tests - one with a bubble and one without, as show in figure 2-2.

Two measurement systems provided parallel data collection for each test that was conducted: pressure data and video data. A Kistler 6052C piezoelectric pressure transducer mounted in the wall of the combustion bomb measured pressure. A Kistler 5010A charge amplifier was used in its most sensitive mode (0.1 bar/ Volt) to amplify the pressure signal. A LABview data acquisition system recorded the pressure at a rate of 5 kHz. The total combustion event took less than one second, making the small amount of drift inherent in the charge amplifier irrelevant.

In addition to the pressure data, each test was also analyzed using Schlieren video data. There were two quartz windows (50.8 mm diameter) on opposite sides of the bomb that gave a direct view of the combustion process. Schlieren videos use a system of collimated light, lenses, and apertures to visualize temperature and density gradients in the gases inside the bomb. This provided an invaluable method of observing the flame front as it propagated through the bomb.

A schematic of the Schlieren setup used in this experiment is shown in Figure 2-3.

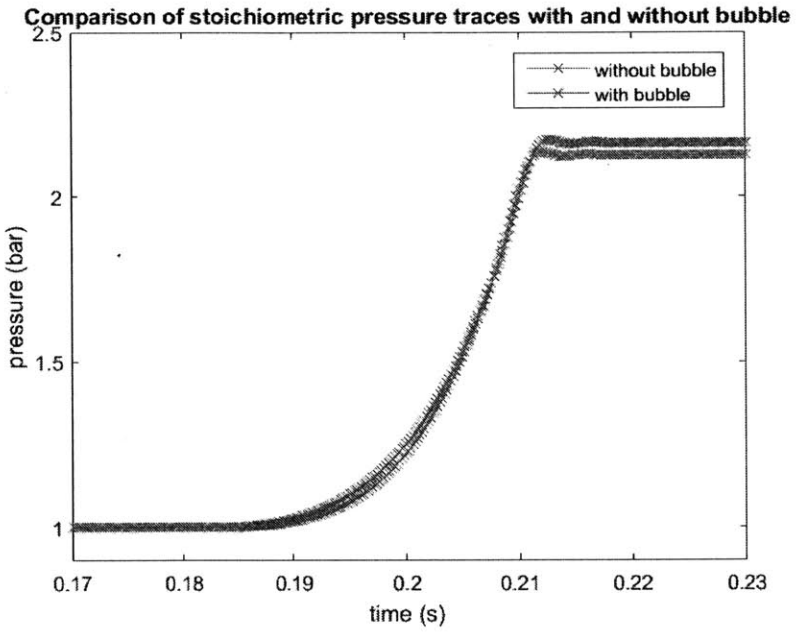

Figure 2-2: The pressure trace of a stoichiometric homogeneous mixture compared with the pressure trace using stoichiometric mixture both inside and outside the soap bubble.

The light that creates the image originates at the arc lamp light source, a UVP model LH-371Q. A small iris in front of the arc lamp provides control over the size of the original light image that is manipulated by the Schlieren system. This beam of light can be thought of as an infinite set of diverging bundles of light; two representative such bundles are shown in figure 2-3. This divergent beam hits a plano-convex lens that converts each bundle into a parallel beam. This set of parallel light bundles enters the combustion bomb through one of the quartz windows, where it encounters the flame front. The burned gas has a significantly different index of refraction than the colder gases. This density gradient at the flame front causes some of the light to be diverted more or less than the rest. After the light exits the bomb via the other window, it passes through another plano-convex lens which refocuses it to a spot approximately the same size as the opening of the small iris. However, before the light is captured by the camera, it passes through another iris which blocks an outer ring of the beam. This means that light that has passed through the flame front, and thus has been diverted from its original path significantly, will not reach the camera. This makes the flame front darker than the rest of the image, and therefor visible.

The image was capture by a high speed camera, a Vision Research Phantom v4.2, which produces 352 x 384 pixel grayscale images at a rate of 2252 Hz. The processing of these images is discussed in section 2.3. An example image is shown in figure 2-4. The system was sensitive enough to reliably capture a fair amount of detail in the flame front.

In order to capture synchronous data from these two sources– the high speed camera and the pressure transducer – a single signal generator box was set up to synchronously provide the necessary trigger signals to the two measurement systems as well as the laser. However, there was some unavoidable variation in the time between when the laser received the trigger signal and when the laser actually lased. As a result, the triggering system was effective only in ensuring that data was recorded during combustion by each system, rather than providing exact synchronization between them.

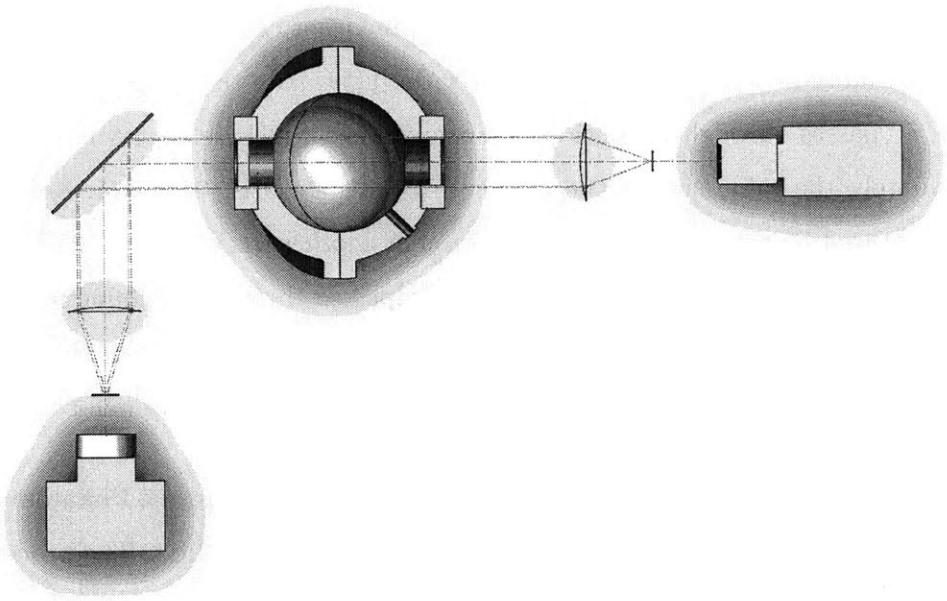

Figure 2-3: The Schlieren system is setup as shown in this schematic: Light originates at the arc lamp in the bottom left corner, passes through a small iris and a plano-convex lens, is bounced off a mirror, enters the combustion chamber where is may or may not be deflected by density gradients, passes through another plano-convex lens, passes through a restricting second iris, and is capture by the high speed video camera pictured on the far right.

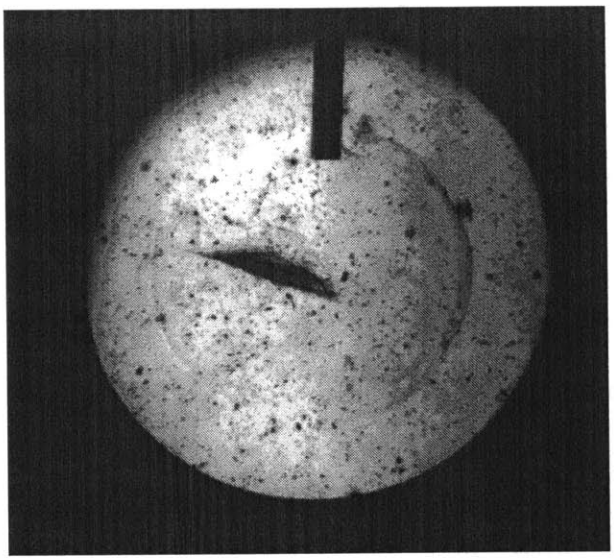

Figure 2-4: The flame front is visible is this sample Schlieren image as a faint roughly circular edge. The straw is also visible as the black rectangle at the top.

2.2 Pressure Data Analysis

Because the purpose of the experiments was to investigate the response of the laminar flame speed to changes in the stoichiometry, the critical piece of analysis was the determination of flame speed. The flame speed was calculated by two different methods, which, in general, agreed quite well. The first method used the pressure trace to extract the flame speed, while the second method analyzes the high speed video. This section details the first method.

2.2.1 Preprocessing and Framework of Assumptions

The pressure inside the bomb was measured at 5 kHz. A sample pressure trace from a test with no bubble (i.e. fully homogeneous mixture) at an equivalence ratio of 1 is show in figure 2-5. The raw pressure trace was noisy enough that it required spectral filtering. A butterworth filter was used, and applied both forwards and backwards to cancel any phase change it might induce. The butterworth filter was of the 6th order with a normalized cutoff frequency in the range of 0.03 to 0.1 of the Nyquist frequency. This range represents the optimal zone in the trade-off between noisy pressure traces (and therefore noisy flame speed data) and unacceptably large deviations between the raw data and the filtered data.

Once the pressure data has been smoothed by filtering out high frequency noise, it was possible to work out the flame speed. This analysis involved several assumptions:

- The gases were assumed to start out as quiescent, at uniform temperature, and having total homogeneity of composition within each of the two different mixtures.
- Any heat or mass diffusion between the two different mixtures, or between the burned and unburned gases, was neglected.
- Any heat transfer by radiation was ignored.
- The bomb walls were treated as adiabatic.

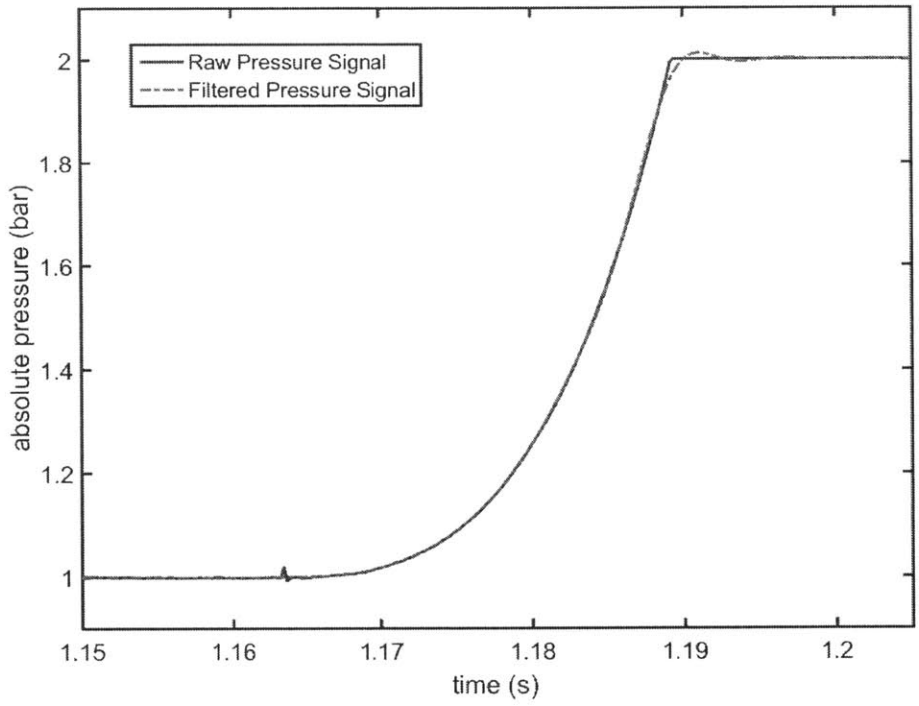

Figure 2-5: This sample pressure trace shows the original and filtered pressure signal. The pressures reach that maximum at about 2 bar not because this was the maximum pressure in the chamber but because the charge amplifier was at a very sensitive setting, meaning it was saturated at about 2 bar.

- The laser was considered to be an ideal and instantaneous ignition source.
- It was assumed that the only chemical reactions that occur happen in a flame front of negligible thickness, and thus burned and unburned gases had time-invariant compositions.
- It was expected that all processes maintain mechanical equilibrium and thus the pressure is at all times uniform.
- The analysis was valid only insofar as buoyancy effects of the less dense burned gases were not yet important.
- Each gas was modeled as an ideal gas.

By introducing this framework of assumptions, the flame speed calculation became fairly straightforward. The strategy involved three steps: calculation of gas properties at each point in the pressure trace, introduction of an assumed flame geometry, and then computation of the flame speed.

2.2.2 Finding Gas Properties

During the first stage of combustion, before the flame front has encountered mixture 2, the gases can be divided into three regions as shown in figure 2-6: the burned gases of mixture 1, the unburned gases of mixture 1, and the entirely unburned mixture 2.

For a given pressure data point, the thermodynamic state of the two unburned gases could be fully determined by assuming isentropic compression from the initial state and solving equation 2.2.

$$\int_{T}^{T_0} \frac{c_p}{T} dT = \frac{\mathbb{R}}{MW} \cdot ln(\frac{P}{P_o}) \tag{2.2}$$

This computation can be done using prepackaged programs like Cantera or using the JANAF tables. The burned gas temperature was calculated as the adiabatic flame temperature at the given pressure level of mixtures 1 and 2 respectively. This represented a significant simplification because the burned gases were not all at a

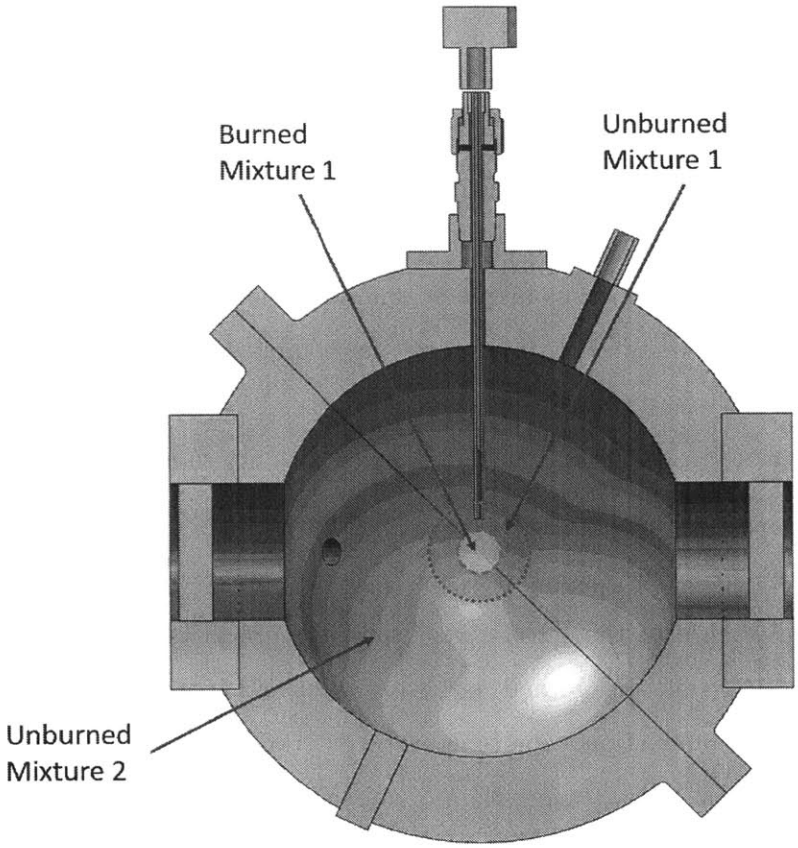

Figure 2-6: The combustion before flame reaches interface is modeled as three regions of gas: the burned gas of mixture 1, the unburned gas of mixture 1, and the entirely unburned mixture 2 gases.

uniform temperature. A higher fidelity model would require considering a series of shells of burned gases at different temperatures as combustion progresses.

With the temperatures of each of these three regions and the pressure (which is the same throughout), the thermodynamic state was fully determined. Using conservation of energy and the volume constraint of the chamber, the fraction of mixture 1 that had burned, $x_{1,b}$, can be calculated as shown in equation 2.3.

$$x_{1,b} = (\frac{p * V_t - N2 * \mathbb{R} * T_{2,u}}{m_1 * \mathbb{R} * T_{1,u}/MW_{1,u}} - 1) * (\frac{T_{1,b} * MW_{1,u}}{T_{1,u} * MW_{1,b}} - 1)^{-1} \tag{2.3}$$

The flame reached the interface when the burned mass fraction of mixture 1 reached unity. It was assumed that there was no mixing between the regions, and thus all points of the flame front arrive at the interface simultaneously. The flame then begins burning through mixture 2, and the bomb's volume can be divided into three new regions: the entirely burned gases of mixture 1, the burned gases of mixture 2, and the unburned gases of mixture 2. These regions are shown in figure 2-7.

An analogous set of calculations was made in this regime. The temperature of the unburned gas of mixture 2 was found assuming isentropic compression (see equation 2.2). The temperature of the burned gas from mixture 1 was found by assuming that the composition of this burned gas was frozen and it was simply compressed isentropically after combustion. The temperature of the burned gas of mixture 2 was taken as the adiabatic flame temperature of this mixture at the given pressure. The mass fraction of mixture 2 that is burned is then determined by equation 2.4

$$x_{2,b} = (\frac{P * V_t - P * V_1}{m_2 * \mathbb{R} * T_{2,u}/MW_{2,u}} - 1) * (\frac{T_{2,b} * MW_{2,u}}{T_{2,u} * MW_{2,b}} - 1)^{-1} \tag{2.4}$$

The burned mass fraction would, ideally, increase until it hits unity when all the gases in the bomb have combusted. In reality, some amount of heat transfer out of the bomb may invalidate the adiabatic assumption that enabled these calculations. However, the flame front hit the interface and transitioned fully into mixture 2 well before these other phenomena became significant.

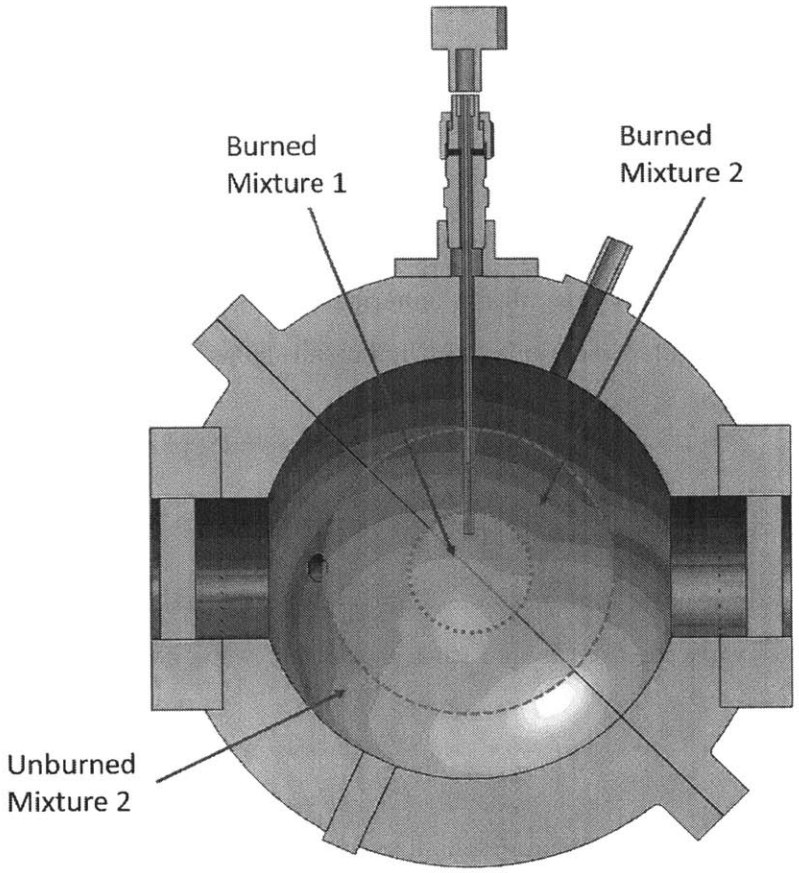

Figure 2-7: The combustion after flame reaches interface is modeled as three different regions of gas: the burned and then compressed gas of mixture 1, the unburned gas of mixture 2, and the unburned mixture 2 gases.

2.2.3 Computing Flame Speed Assuming Sphericity

Using the pressure to find the thermodynamic states of each region of gas necessitates the assumption that the flame is always burning either mixture 1 or mixture 2, rather than part of the flame front being in mixture 1 and part in mixture 2. This assumption does not imply that the flame front is spherical until the flame hits the interface. However, to find the flame speed from the burned gas fraction, the spherical assumption must be made explicitly. The governing equation for the flame speed is given in equation 2.5.

$$\frac{dm_{1,b}}{dt} = S_L * A_f * \rho_u \tag{2.5}$$

In order solve this equation, the flame front's area must be known. Thus we assumed that the flame front was always spherical. This was a key assumption that will be discussed in detail in section 4.2. If the flame is spherical, the flame speed can be calculated as shown in 2.6.

$$S_L = \frac{m_1}{4\pi r^2 \rho_u} * \frac{dx_{1,b}}{dt} \tag{2.6}$$

The r in eq 2.6 is the flame radius. This value is the main result of the video analysis, but it can also be determined from $x_{1,b}$ and ρ_b using equation 2.7.

$$r = \left(\frac{m_1 * x_{1,b} * \mathbb{R} * T_{1,b}}{MW_{1,b} * 4/3\ \pi * P} \right)^{1/3} \tag{2.7}$$

Altogether this analysis determines the flame speed over the course of the flame's propagation.

2.3 Video Data Analysis

In addition to calculating the laminar flame speed from the pressure data, the flame speed was also determined using the high speed video. Each combustion event was recorded in a series of 352 x 384 pixel images taken at 2252 Hz. The camera records in traditional 256-point grayscale. A typical image showed the flame front at a grayscale

intensity of about 60 compared to lighter areas around it with intensity around 100 on the grayscale. This difference was exploited in a code developed in-house that determined the edge of the flame front in each frame. This algorithm for tracking the flame front (and then calculating the flame speed) demonstrated good correlation with the pressure data analysis, though it is only possible during the initial stages of flame development before the flame front disappears from the view (because of the limited field of view through the windows in the bomb). Nevertheless, by making the video analysis automated rather than manual, the calculation speed was dramatically increased and the influence of human error reduced. This section provides details on the algorithm used to define the flame front in each image, and to calculate the flame speed from this data.

2.3.1 Preprocessing

The video analysis required some initial preprocessing done by hand. Essentially the main processing code needed some initial conditions. The user had to define the flame front in the first viable frame of the video, and then the code could determine the flame front's location in the subsequent images. The first viable frame is simply the first frame where the flame front is visible enough for a user to select the points in the image which define it. The entire edge of the flame front does not need to be well-defined, just enough of its edge to fit an oval: around 10-15 points that define at least around half of the flame front would suffice. A sample of this preprocessing is shown in figure 2-8. The oval fitted to these points is assumed to be the center of the flame ball, and it was assumed that this point remained constant throughout the combustion process captured on video.

2.3.2 Automated Processing

Once the flame front's position in an initial frame has been specified by the user, the flame's location could be determined in each subsequent frame. This process occurred in five main steps:

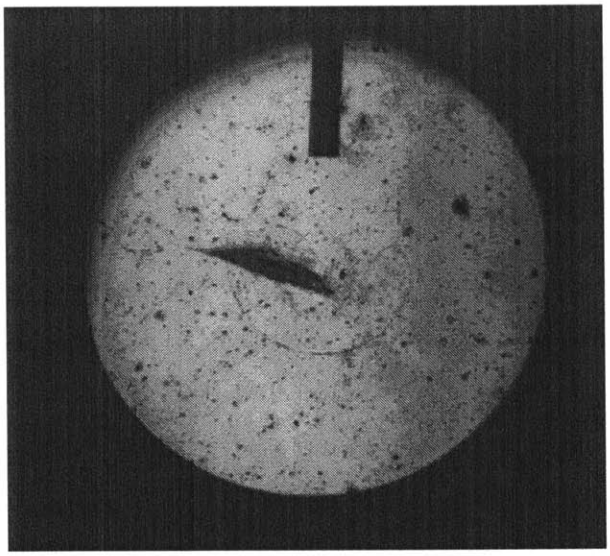

Figure 2-8: Example of the manual fitting of points to the initial flame front in one of the first few frames of the video. Pink x's show manual input selections of the flame front. The remainder of the now burst bubble is also visible in this particle image.

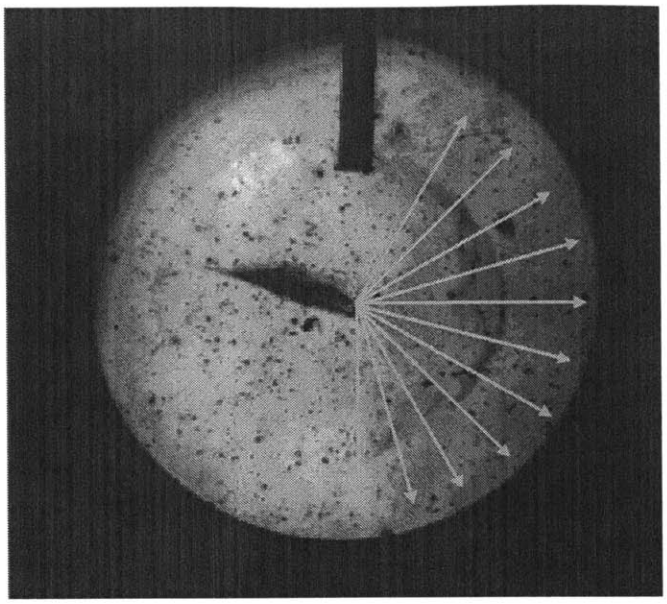

Figure 2-9: Example of the search paths along which the algorithm finds points that define the edge of the flame front in a given frame.

1. Search paths were defined along which the code will look for the flame front in a given frame. These paths were sets of pixels that form lines outward from the center of the flame front, as it had been defined by the user input in the preprocessing phase. These paths are shown in figure 2-9.

2. Each image had the following image subtracted from it. This is a "moving" background subtract. Typically a background subtract is used to eliminate constant features in a video that are not of interest. In these videos, those features are things like the straw, or the spots generated by lens imperfections. However by using a moving background subtract, it was possible to also eliminate features such as bubble remnants (or slow-moving portions of bubble remnants) that may move throughout the video but are not features of interest.

3. Each image was converted from grayscale to black and white. The goal here was to define the flame front as a set of white points on a black background. The conversion mechanism imposed a threshold value for what is considered white versus black in the new binary image. For example, if the threshold value was

80, then any pixel with a value of 79 or below was made into a 0, while pixels at 80 or higher were converted to 1's. The Otsu method, which attempts to minimize variation of intensity within the black and white classes, was used to find this threshold value. [18,19]

4. For each frame, the code searched for white pixels that fell on the search paths from step 1. If a white pixel is found on a given path, it's location was a "hit" for that frame. The collection of hits in one frame defined the flame front at that instant. The search is subject to a few constraints. A hit was required to fall within a given range on the search path relative to the flame front's location in the previous frame, or, if there was not a hit on that search path in the previous frame, relative to the code's guess of where the flame was in the previous frame. If multiple white pixel meet the criteria, the outermost one is chosen. Figure 2-10 shows the progression of these image processing steps for one frame in a video.

5. The radius of the flame, in each search direction, for each frame, was the difference between the relevant hit and the original center point. This calculation assumed that the flame was propagating normal to each search path, or spherically, which is not strictly true. However, the method presented above, and an analogous method that considered changes in flame radius along a local normal vector were found empirically to produce the same result. This justifies the employment of the radial propagation, which was used because it was faster computationally.

This set of flame radii, with several measurements for each frame, was the key output of this process. The data could be compared to the radii calculated from the pressure data, or could be used to make an estimate of flame speed as a function of time.

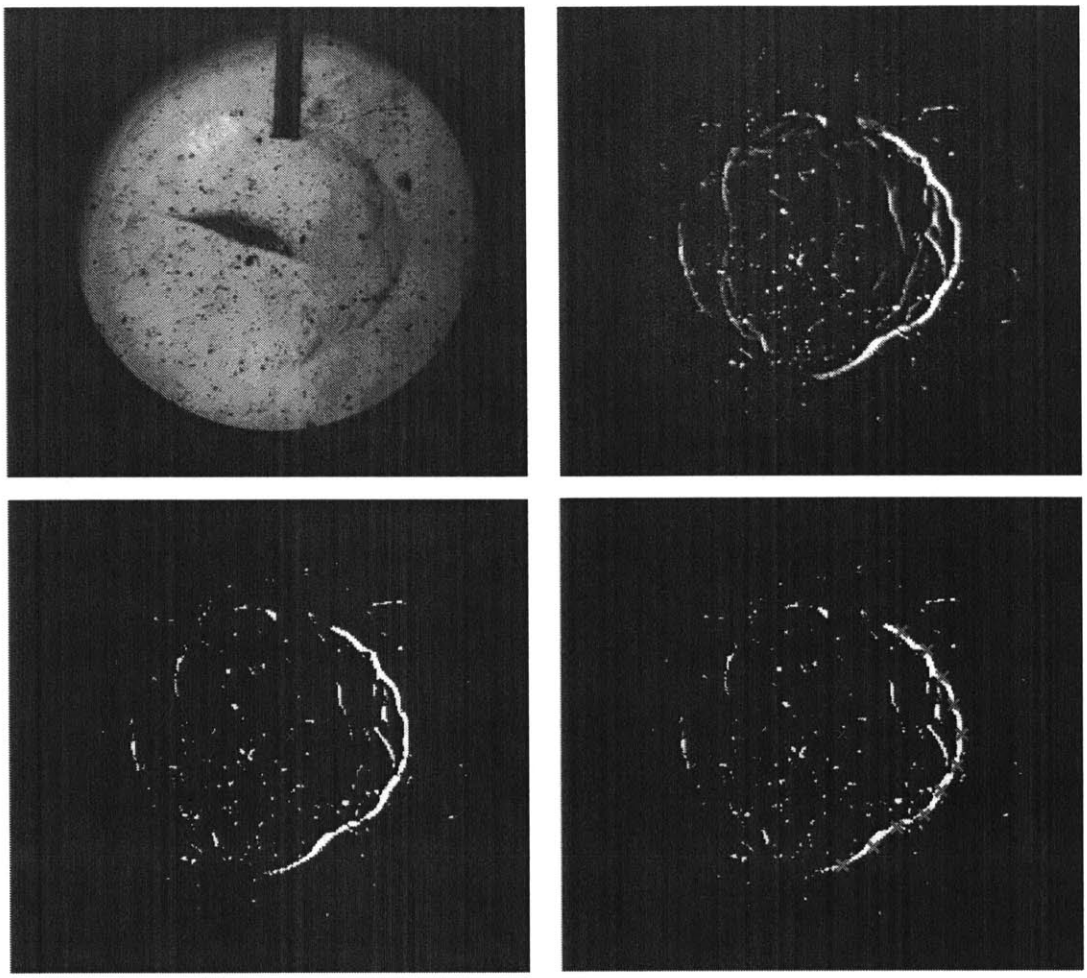

Figure 2-10: Sequence of image processing steps performed by the image processing GUI. The original image is shown on the top left. The top right shows that same image after the background subtract (and some contrast enhancement). The bottom left image shows the black and white version, and the bottom right shows the matched flame front points over the black and white image. The slightly wrinkled flame front is a result of the flow field perturbation by fragments of the bursted soap bubble.

2.3.3 Estimate of Flame Speed

While it is useful to compare the video-determined flame radii to the pressure-determined flame radii, it's also possible to compare the flame speed from these two measurement systems. However, to convert the flame radii to a flame speed, it's necessary to estimate the ratio of the densities of the burned and unburned gases, as shown in Eq. 2.8, where S_l is flame speed, and r_{flame} is the flame radius.

$$S_L = \frac{\rho_{burned}}{\rho_{unburned}} * \frac{d\,r_{flame}}{dt} \tag{2.8}$$

For Eq. 2.8 to hold, the flame must be propagating spherically and the local burned gas velocity must be zero in the laboratory reference frame. It turned out that this was not true most if not all of the time. The high speed video shows that the flame front develops a large protrusion on one side (the left side in the video images). The likely reasons for this phenomenon and its effects are discussed in section 4.2.

2.3.4 Control of Video Processing Via GUI

A simple graphical user interface (GUI) was created to facilitate user control of the video analysis process. The idiosyncrasies of each test required slight adjustment in some video processing parameters. An image of the GUI is shown in figure 2-11. The program allowed for user control in the following ways:

1. While the Otsu method of determining the appropriate threshold for image conversion to binary worked well in most cases, sometimes a different level better captured the edges of the flame front. The user could directly change the threshold value via the GUI.

2. Because the flame is not spherical, generally the right hand side (as shown in figure 2-11) was much better for tracking the flame radius since the protrusion was always on the left. The GUI allowed the user to select the angular range of the flame front best suited for tracking.

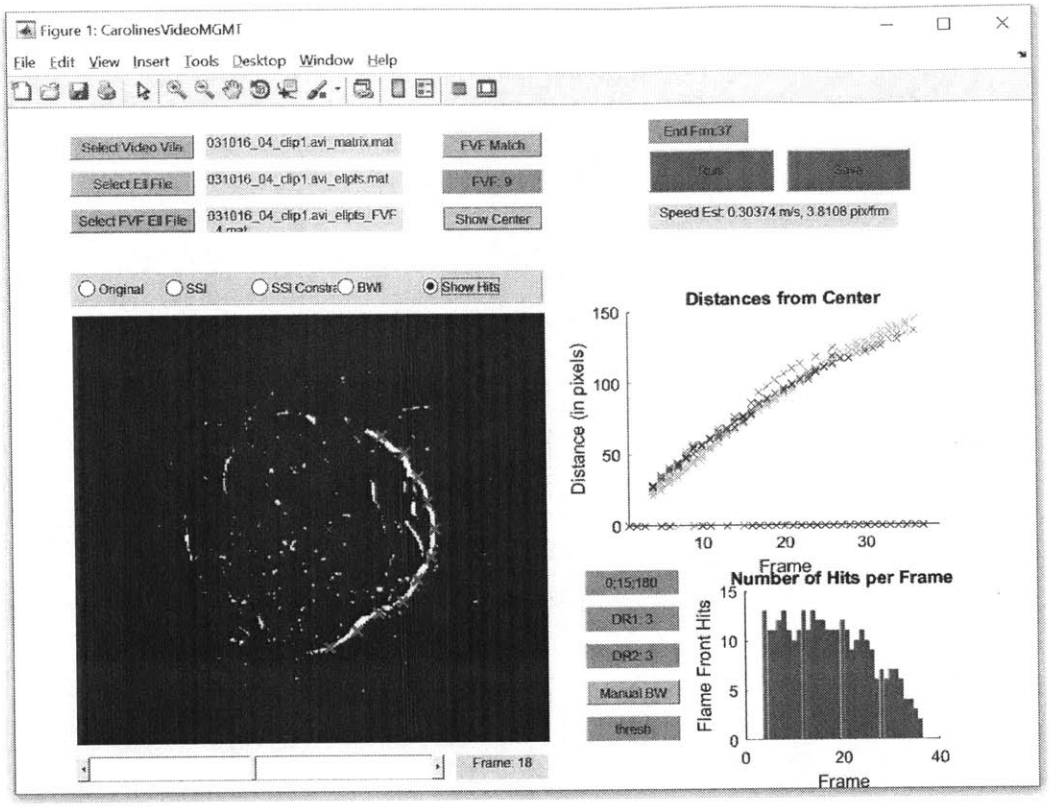

Figure 2-11: Screenshot of the GUI showing a frame in the Schlieren video, and the points (red x's) that the algorithm has found that define the flame front in that frame. The scatterplot on the right hand side shows the flame radius for the points that the GUI finds. The bar graph below it in red shows how many points have been found per frame (generally between 5 and 10).

3. The Schlieren video was far from perfect at capturing a fully-defined flame front. The GUI would not interpolate points, but it would provide some user adjustment in defining the range (relative to the previous flame front point) along the search path that would be a valid location for the current flame front.

Chapter 3

Results

This section presents the results of two main classes of tests: the homogeneous case where there was no bubble and the whole bomb was filled with one mixture, and the stratified case where a soap bubble was used to separate two mixtures.

3.1 Homogeneous Case

The homogeneous tests were important in validating the experimental process and the data analysis. Tests were conducted using a wide range of equivalence ratios for both propane and methane. These tests were analyzed using the pressure data and the video data.

3.1.1 Pressure Trace Results

There pressure data analysis calculated two interesting pieces of information: the first one was the flame radius over time, and the other was the flame speed. Figure 3-1 shows the development of the mass fraction burned, the flame radius, and the flame speed, for the case of stoichiometric methane air mixture. The flame speed is zero before ignition, then briefly spikes, and then settles to a stable value. Eventually the apparent flame speed will drop because of heat transfer out of the bomb and because of buoyancy effects. The initial spike is partly due to the energy deposition from

the laser, and party to the high rate of flame stretch rate in the first moments of propagation. The flame stretch rate can be calculated according to equation 3.1.

$$\kappa = \frac{1}{A_f}\frac{dA_f}{dt} \tag{3.1}$$

If the flame is spherical, and only flame stretch due to curvature change is considered, equation 3.1 reduces to 3.2

$$\kappa_c = \frac{2}{r_f}\frac{dr_f}{dt} \tag{3.2}$$

Thus the stretch rate is appreciable only when the radius is small. The stretch rate itself can be used to relate the stretched (or measured) flame speed to the unstretched flame speed according to eq 3.3. The Markstein length, $\mathscr{L}$, for a given value of κ_c can be found from numerical correlations published by Bradley [20]. By the time the flame ball has a radius on the order of 1 cm κ_c is below 100 1/s, and therefore flame stretch is insignificant. The critical stretch value (where stretching effects are not only important but dominant) is when $\kappa_c \sim S_L^2/\mathcal{D}$, or about 10^4 1/s.

$$S_{L,unstreched} = S_{L,streched} + \mathscr{L}\kappa_c \tag{3.3}$$

By using this pressure trace analysis, it was possible to measure flame speeds for methane-air mixtures in a range of equivalence ratios. The results were in good agreement with other published values. Figure 3-2 shows the results of this experimental work (using the pressure trace analysis) as compared with a few other studies [21–24].

One other unexpected feature that was observed in a majority of the recorded pressure traces was a small, short increase and then immediate decrease in the pressure trace right before the flame propagation began. The magnitude of this feature was around 500 Pa above and then below the local average pressure. The spike consisted of a single data point, and if there was a subsequent decrease it was always the immediate next data point. It is hypothesized that this was a pressure wave, generated by the near-instantaneous ignition process, registering in the pressure transducer. Further evidence of this hypothesis can occasionally be seen in the Schlieren video. Rarely,

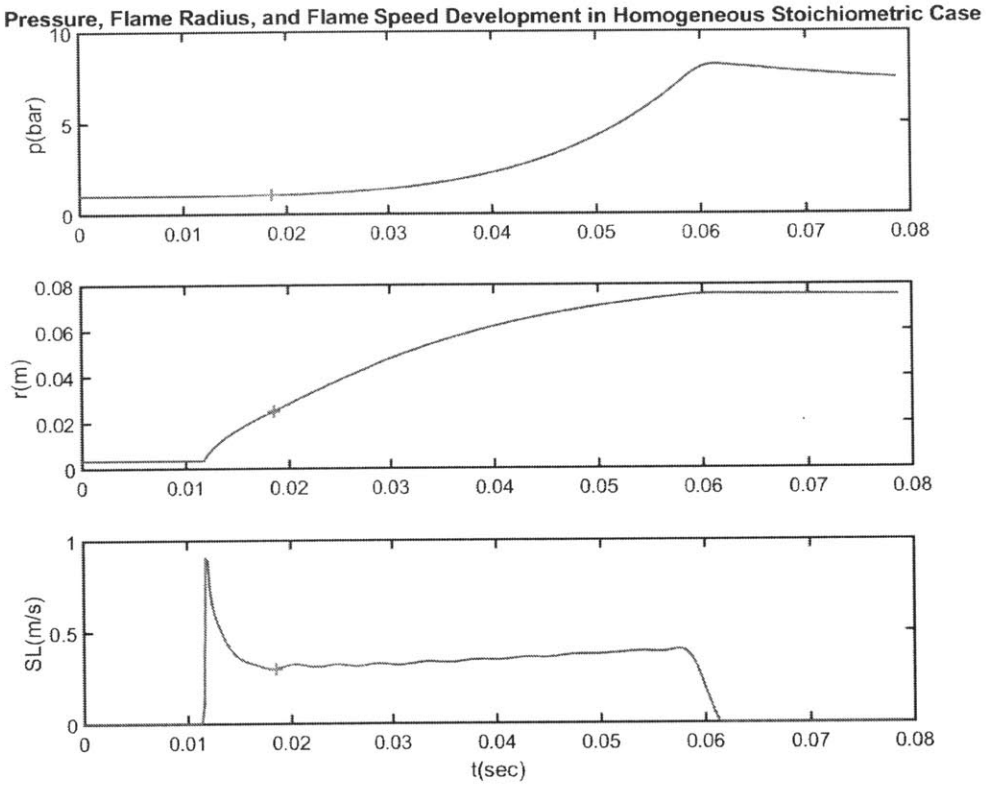

Figure 3-1: Flame development as calculated from pressure trace in a homogeneous charge of stoichiometric methane and air.

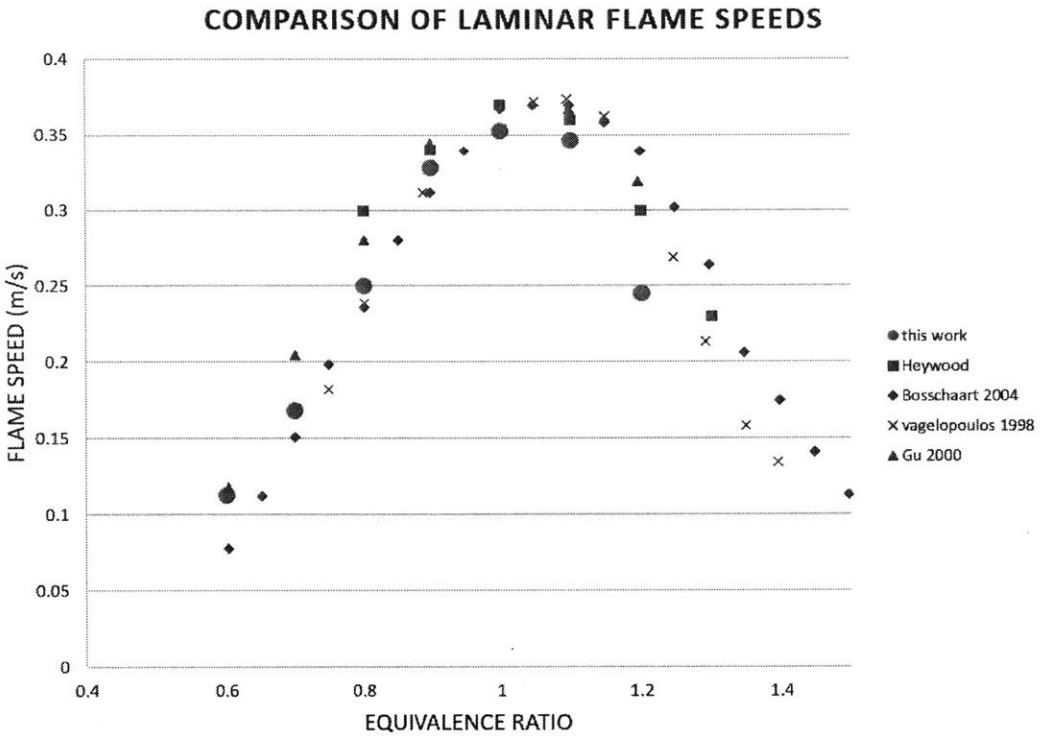

Figure 3-2: Flame development as calculated from pressure trace in a homogeneous charge of stoichiometric methane and air.

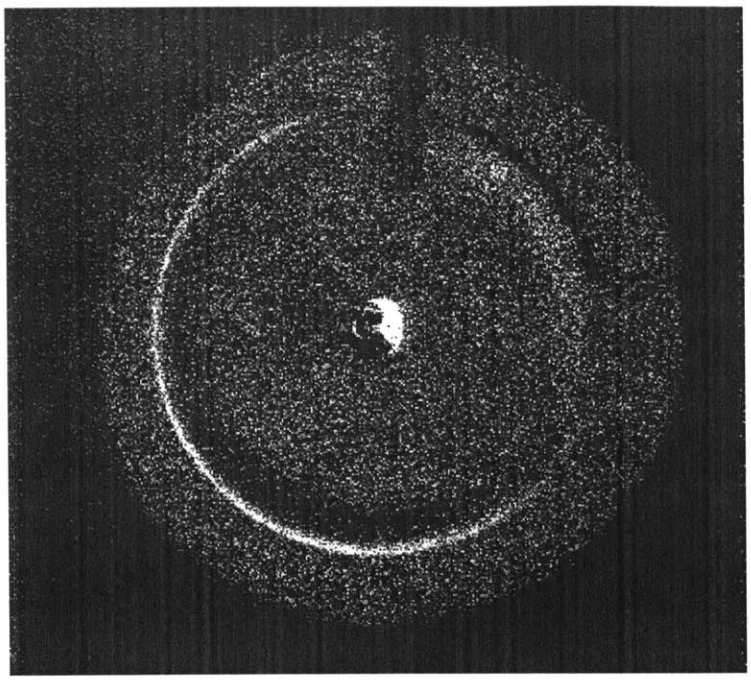

Figure 3-3: The presence of an unexplained spherical density gradient is hypothesized to be a low-magnitude shock wave from the ignition process. The flame kernel is shown as the mainly white feature at the center of the image. The large and very spherical white curve is the possible pressure wave.

but on several occasions, an unexpected density gradient is observed in the first frame after ignition. This circular density gradient is clearly not the flame front because it appears for only one frame at an arbitrary radius. The possible shock wave is very faint in the original video, but becomes clear with an increase in contrast. An example is shown in figure 3-3.

3.1.2 Video Results

The high speed Schlieren video was also used to measure flame radius. From this flame radius and the gas properties calculated from the pressure trace, the flame speed was

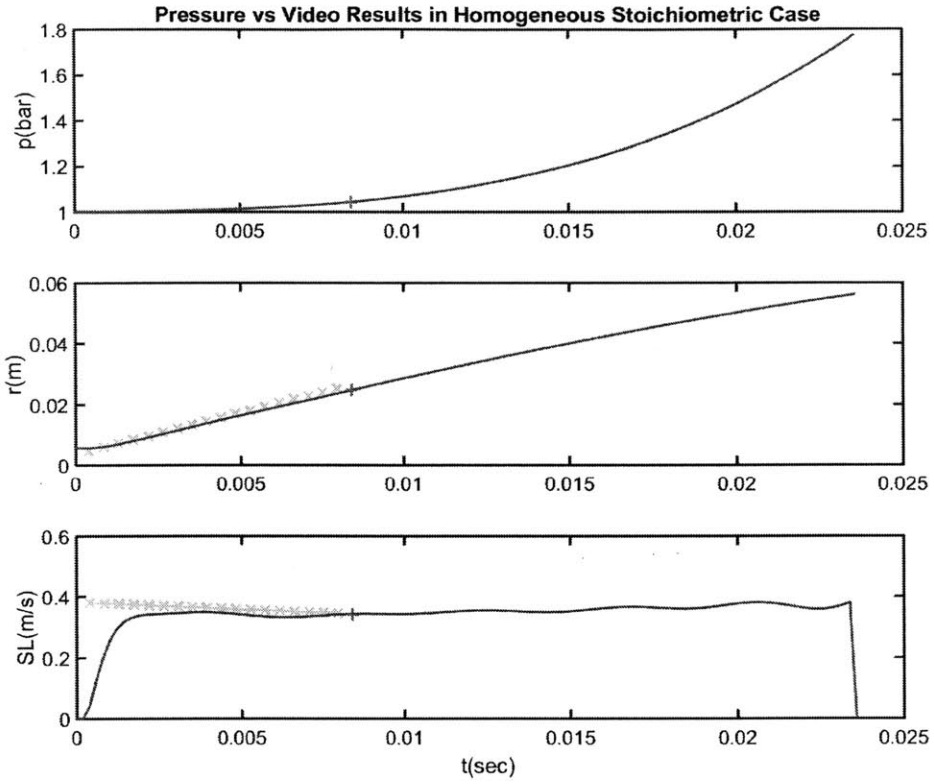

Figure 3-4: Flame development as calculated from pressure trace and video data in a homogeneous charge of stoichiometric methane and air.

calculated. There was in general good agreement between the flame radius detected in the video and the flame radius calculated using the pressure. The video-derived and pressure-derived flame speeds also matched well. Figure 3-4 shows the same data as figure 3-1, but with the addition of the video-derived data.

3.2 Stratified Case

The stratified experiments had unexpected results. Experiments were carried out using a range of equivalence ratios for both mixtures 1 and 2. The anticipated strategy of measuring the transition from the flame speed characteristic of mixture to that of mixture 2 once the flame hit the interface was complicated by the fact that the

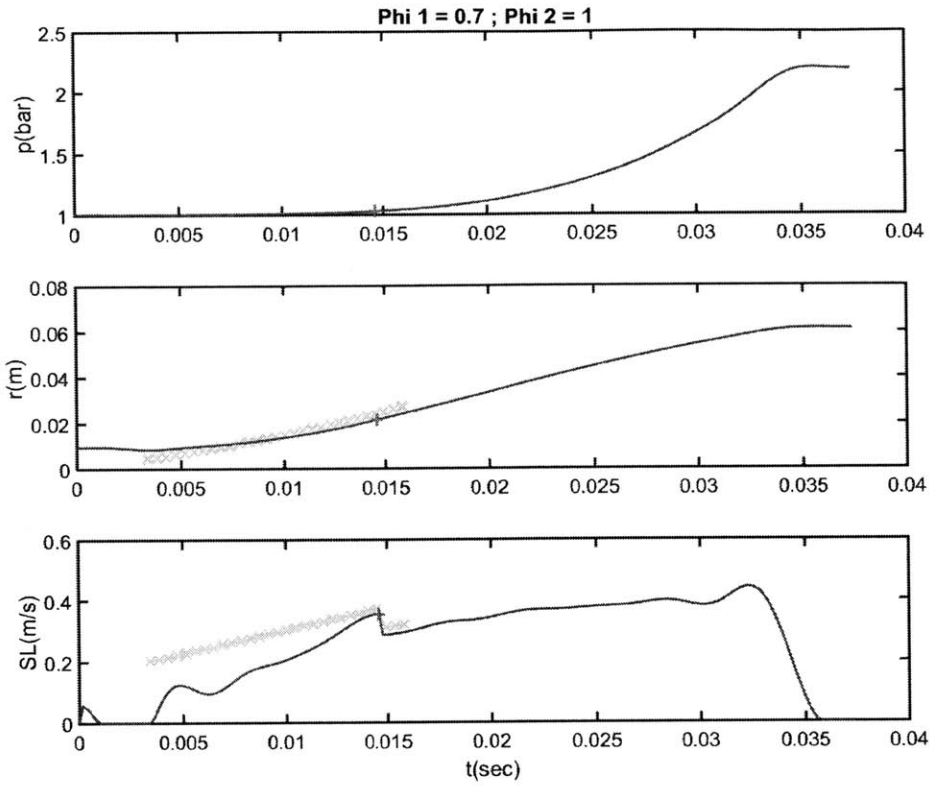

Figure 3-5: The transition of flame speed from mixture 1 with phi 0.7 to mixture 2 with phi 1. The small, pink crosses mark the point when the flame is calculated to cross the interface.

flame speed appeared to begin transition well before reaching the interface. This phenomenon is demonstrated in figure 3-5.

The sharp change in flame speed in figure 3-5 shows the effect of the changing density ratio. However, the flame speed up until that point is almost perfectly linear. This was surprising. It was expected that the flame speed would be stable until it reached the interface and would then begin transitioning to the flame speed of mixture 2. Both the pressure trace results and the video results show that this is not what is happening. This slow, linear, early transition was observed across the range of equivalence ratios. It is more or less pronounced depending on the difference in equilibrium flame speed of the two mixtures. For example, in the case where mixture

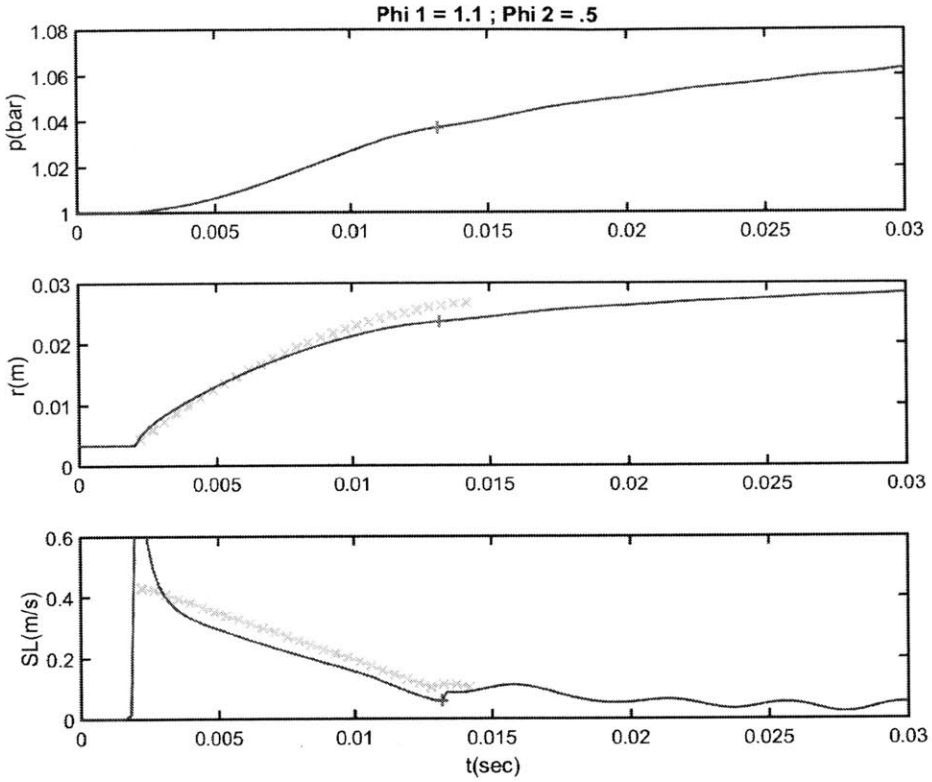

Figure 3-6: The transition of flame speed from mixture 1 with phi 1.1 to mixture 2 with phi 0.5. The small, pink crosses mark the point when the flame is calculated to cross the interface. The flame speed never stabilizes at the homogeneous-case speed of phi 1.1.

1 has equivalence ratio of 1.1, meaning a relatively high flame speed, and mixture 2 has a 0.5 equivalence ratio (just below the measured lower flammability limit), the flame speed begins descending immediately (see figure 3-6).

Section 4 suggests possible reasons for these surprising results.

Chapter 4

Discussion

The strategy that was employed to measure flame speed over step changes in stoichiometry was not successful. As was discussed in 3.2, the flame speed began transitioning from one flame speed to another significantly before it reached the expected location of the interface. This suggests that the original premise of a sharply stratified charge did not hold. This surprising finding is largely attributed to the protrusion that extends from one side of the flame ball, making it non-spherical. This section presents the thinking behind this conclusion.

4.1 Homogeneous Case

The results of the homogeneous, no-bubble tests validated the overall measurement systems and data analysis. The flame speeds that were measured demonstrate that the general approach was sufficient if stratification is not in play.

4.2 Stratified Case

The behavior of the flame speed suggests that the sharp interface created by the bubble between the two mixtures did not result in all points on the flame front simultaneously reaching a sharp interface. This section will discuss two hypotheses that may have created this result. First, it is hypothesized that between ignition

and the time when the flame reaches the interface, there was enough mixing that the interface was no longer a sharp but rather was a smooth gradient. Second, it is hypothesized that the protrusion visible in the video reached the interface before the rest of the flame, resulting in a long period of time during which more and more of the flame front crosses the interface. This second hypothesis, that the protrusion contaminated the pressure and video data results, fits with the observed data, while the first does not align with some key observations.

4.2.1 Mixing in the Stratified Case

One hypothesis to explain the slow, early flame speed transition is mixing. Specifically, mixing could occur in two ways: first, the breakup of the bubble once it bursts sends soap fragments into chaotic movement which could produce bulk mixing; second, there could be diffusional mixing between the stratified layers in the time between ignition (when the bubble bursts) and when the flame reaches the interface. Both of these mixing hypothesis are rejected.

The videos show significant bubble fragment movement throughout combustion. The movement is not repeatable, nor is the size of the soap fragments. Therefore, if these soap pieces were causing mixing, it would be nonuniform and inconsistent from test to test. Such mixing would cause variable flame speed across the flame's area, which would create a wrinkled flame front. This is not observed in the video. Although the flame eventually turns cellular, this occurs far too late in the progression of the flame to be an effect of the bubble fragments.

The possibility of diffusional mixing was also considered. The thickness of the diffusional mixing layer is estimated from equation 4.1 .

$$L_{diff} \sim \sqrt{\mathcal{D}t} \tag{4.1}$$

Given that the flame reaches the interface within about 10 ms, and that the diffusion coefficient for methane in air is 0.21 cm^2/s at 298 Kelvin [25], then the diffusional mixing thickness is on the order of a millimeter or less, meaning it couldn't

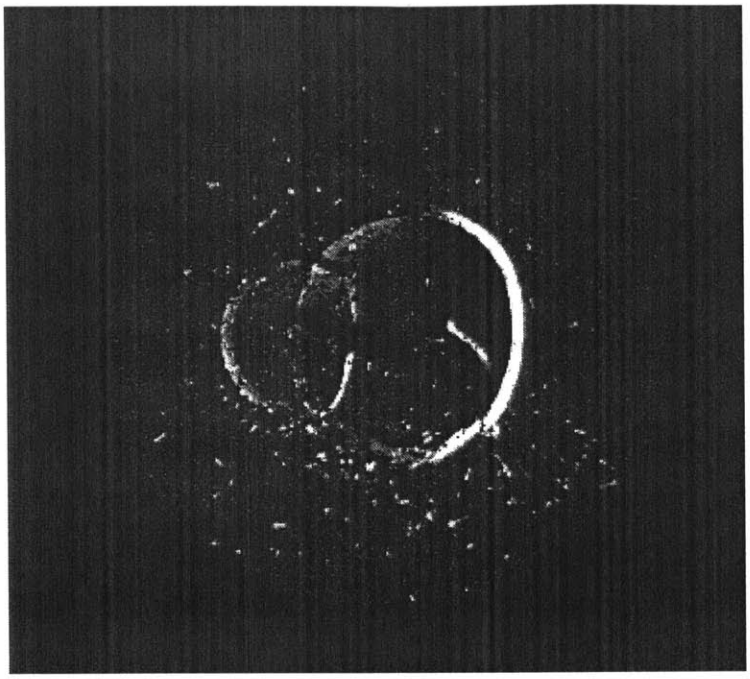

Figure 4-1: An example of the protrusion in the flame front. The protrusion is consistently seen in the location shown. It may vary in magnitude but not in location. The image has been processing using a background subtract and contrast enhancement to make the protrusion clearer.

account for the long transition time.

4.2.2 Effects of the Flame Front Protrusion in the Stratified Case

The second hypothesis that explains the flame speed development concerns the protrustion in the flame front that is observed in the Schlieren video.

This lobe protrudes from the main quasi-spherical flame front to varying degrees, but is present in the majority of tests, always on the left side of the frame, as shown in figure 4-1. It is an artifact of the laser ignition system. The laser deposits energy in

a small parcel of gas at the center of the bomb, but the distribution of energy within this small oblong volume of gas is not uniform. Because of beam attentuation along its pathway, the portion of gas closer to the laser source absorbs more energy than the farther section does. This gradient in energy affects the gas dynamics resulting in the non-spherical shape of the flame front, as was observed by Morsy [15] and Bradley [16]. The experiments of Morsy [15] also showed a somewhat flattened right hand side and a significant protrusion on the side closer to the laser as the main non-spherical features of the ignition kernel. This protrusion affected both the pressure and video results.

The pressure analysis assumes that the flame burns all of mixture 1 before it burns any of mixture 2. The protrusion invalidates this assumption and introduces error. If part of the pressure rise is due to combustion of mixture 2, then equation 2.3 is no longer correct. The real mass fraction of mixture 1 that has burned, $x_{1,b}$, depends on the fraction of the flame area that is burning through mixture 2.

This protrusion issue does not affect the homogeneous case for a few reasons. First, the two mixtures are the same composition so there is not difference in the flame speeds. Second, the flame area is not significantly different from the area of a sphere of the same size. This means that the $4\pi r^2$ term in equation 2.6 is a reasonable approximation. Finally, the protrusion's distortion of the flame shape diminishes as the flame area grows.

The video analysis provides only a two dimensional view of the flame propagation, making it impossible to accurately extrapolate the full three dimensional shape of the flame front, let alone precisely determine the exact composition of gases around the protrusion. The result is a smoothing of the transition between the flame speeds characteristic of either mixture, masking the real transition behavior over the interface. This also explains why the flame speed begins transition shortly after ignition since the far edge protrusion hits the interface much before the rest of the flame.

The protrusion also effects the flame speed that is calculated from the video. For example, figure 3-5 shows a very linear increase in flame speed as the flame propagates from mixture 1 with equivalence ratio of 0.7 to mixture 2 with equivalence ratio 1.

A possible explanation goes like this: As the protrusion begins burning mixture 2, there's more heat release than there is from the flame area burning in mixture 1. This could invalidate two assumptions inherent in the video analysis: first, it might create translational movement of the whole flame ball, and second it could cause the more spherical section of the flame ball to be shrunk (or expanded, depending on the equivalence ratio of mixture 2) by the higher pressure outside the flame than what would be expected if only mixture 1 was being burned.

Translational movement of the whole flame ball would likely be mostly in the horizontal direction rather than vertical given the location of the protrusion. It's possible to use the video analysis algorithm strictly on sections of the flame front that are roughly on the top and bottom (up to 30 degrees off the vertical axis) of the flame rather than the side. If translation movement was causing some of the early transition, then measuring only from the top and bottom of the flame front should minimize this effect. Figure 4-2 shows this effect.

Overall the evidence supports the theory that the protrusion causes the unexpected flame speed transition behavior rather than mixing of the gases. The one observation that is not fully in line with this explanation is that while all the stratified tests show the slow, early flame speed transition behavior, not all the videos show a large protrusion. Some videos seems to have very little deviation off sphericity. It is unclear how sensitive the flame speed behavior is to the magnitude of the protrusion. Furthermore, the consistency of the radial position of the protrusion (and thus its visibility in the focus plane of the Schlieren system) is unknown. It's difficult to determine whether the absence of a large protrusion in some videos is merely an result of the two-dimensional image or a signal that the flame speed behavior is dependent on other mechanisms. However, the protrusion is currently the best explanation available for the unexpected progression of the flame speed.

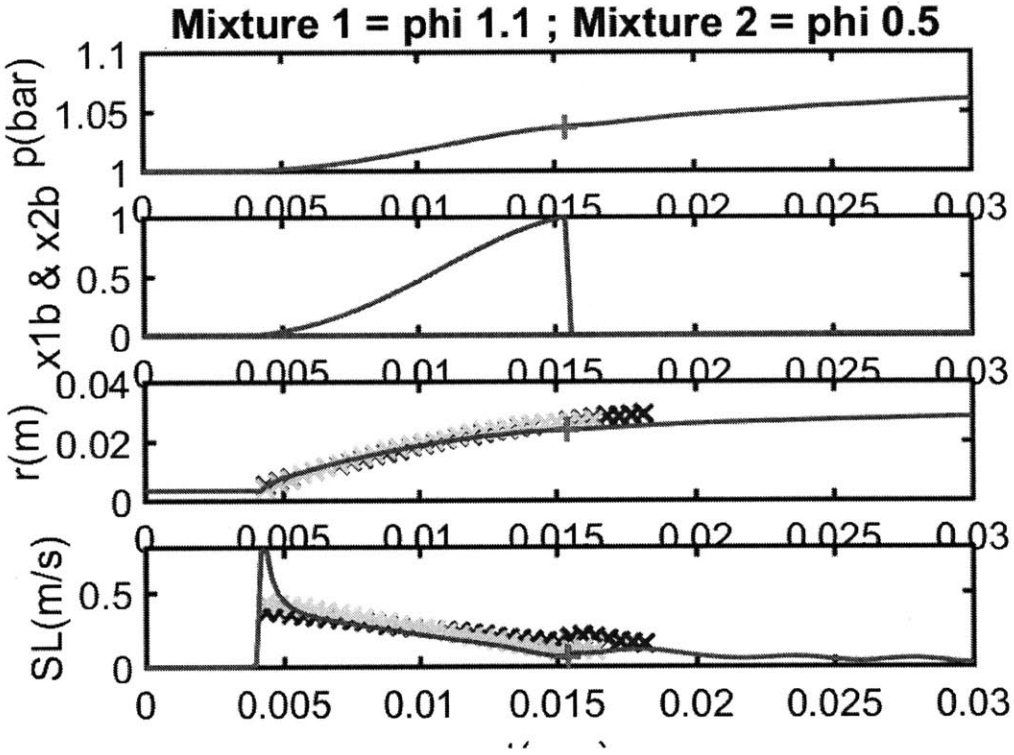

Figure 4-2: This image shows the difference between the flame speed at the top and bottom (blue x's) of the flame ball versus the right side (green x's).

Chapter 5

Conclusions

The motivation for this work was to extend the understanding of flame speed behavior over step-changes in equivalence ratio that was demonstrated by Ra [13]. However in investigating this question using a combustion bomb and the soap bubble method, it became apparent that the effects of the laser ignition system (namely the non-sphericity of the flame front) significantly disturbed the integrity of the step-change paradigm. Because the laser ignition created a protrusion from one side of the flame front, some portions of the flame are reached the interface between the mixtures before the rest. Therefore, while the experiments performed achieved successful flame speed measurement via pressure and Schlieren video analysis for the homogeneous case, it was shown that this setup is not capable of measuring flame speed transitions across step-changes in composition.

Bibliography

[1] Venera Brinzea, Maria Mitu, Codina Movileanu, Adina Musuc, and Domnina Razus. Expansion Coefficients and Normal Burning Velocities of Propane-Air Mixtures by the Closed Vessel Technique. *Analele Universitatii Bucuresti: Chimie*, 19(2):31, October 2010.

[2] A.s. Huzayyin, H.a. Moneib, M.s. Shehatta, and A.m.a. Attia. Laminar burning velocity and explosion index of LPG–air and propane–air mixtures. *Fuel*, 87:39–57, 2008/1/1/2008///.

[3] Domnina Razus, Dumitru Oancea, Venera Brinzea, Maria Mitu, and Codina Movileanu. Experimental and computed burning velocities of propane–air mixtures. *Energy Conversion and Management*, 51:2979–2984, 2010/1/1/2010///.

[4] Ruigang Zhou and Simone Hochgreb. The behaviour of laminar stratified methane/air flames in counterflow. *Combustion and Flame*, 160:1070–1082, 2013/6/1/June 2013///.

[5] Shaoyun Ren and Qi Zhang. Influence of concentration distribution of hydrogen in air on measured flammability limits. *Journal of Loss Prevention in the Process Industries*, 34:82–91, 2015/3/1/March 2015///.

[6] Xinyan Wang, Hua Zhao, and Hui Xie. Effect of dilution strategies and direct injection ratios on stratified flame ignition (SFI) hybrid combustion in a PFI/DI gasoline engine. *Applied Energy*, 165:801–814, 2016/3/1/1 March 2016///.

[7] Xinyan Wang, Hua Zhao, and Hui Xie. Effect of piston shapes and fuel injection strategies on stoichiometric stratified flame ignition (SFI) hybrid combustion in a PFI/DI gasoline engine by numerical simulations. *Energy Conversion and Management*, 98(98):387–400, July 2015.

[8] Xian Shi, Jyh-Yuan Chen, and Zheng Chen. Numerical study of laminar flame speed of fuel-stratified hydrogen/air flames. *Combustion and Flame*, 163:394–405, 2016/1/1/January 2016///.

[9] Jiacheng Zhang and John Abraham. A numerical study of laminar flames propagating in stratified mixtures. *Combustion and Flame*, 163:461–471, 2016/1/1/January 2016///.

[10] Y.m. Marzouk, A.f. Ghoniem, and H.n. Najm. Dynamic response of strained premixed flames to equivalence ratio gradients. *Proceedings of the Combustion Institute*, 28:1859–1866, 2000/1/1/2000///.

[11] Saravanan Balusamy, Armelle Cessou, and Bertrand Lecordier. Laminar propagation of lean premixed flames ignited in stratified mixture. *Combustion and Flame*, 161:427–437, 2014/2/1/February 2014///.

[12] Irfan A. Mulla and Satyanarayanan R. Chakravarthy. Flame speed and tangential strain measurements in widely stratified partially premixed flames interacting with grid turbulence. *Combustion and Flame*, 161:2406–2418, 2014/9/1/September 2014///.

[13] Youngchul Ra. *Laminar flame propagation in a stratified charge.* Thesis, Massachusetts Institute of Technology, 1999.

[14] Phred Petersen. Schlieren and Shadowgraph Photography. *The Focal Encyclopedia of Photography*, pages 610–612, 2007/1/1///.

[15] M.h. Morsy and S.h. Chung. Numerical simulation of front lobe formation in laser-induced spark ignition of CH4/air mixtures. *Proceedings of the Combustion Institute*, 29:1613–1619, 2002/1/1/2002///.

[16] D. Bradley, C.g.w. Sheppard, I.m. Suardjaja, and R. Woolley. Fundamentals of high-energy spark ignition with lasers. *Combustion and Flame*, 138:55–77, 2004/1/1/2004///.

[17] Kewal Dharamshi, Dhananjay Kumar Srivastava, and Avinash Kumar Agarwal. Combustion characteristics and flame-kernel development of a laser ignited hydrogen–air mixture in a constant volume combustion chamber. *International Journal of Hydrogen Energy*, 39(1):593–601, January 2014.

[18] N. Otsu. A threshold selection method from gray-level histograms. *IEEE Transactions on Systems, Man and Cybernetics*, SMC-9(1):62–66, January 1979.

[19] Global image threshold using Otsu's method - MATLAB graythresh. `http://www.mathworks.com/help/images/ref/graythresh.html?requestedDomain=www.mathworks.com`.

[20] D. Bradley, P.h. Gaskell, and X.j. Gu. Burning velocities, Markstein lengths, and flame quenching for spherical methane-air flames: A computational study. *Combustion and Flame*, (1-2):176, 1996.

[21] X.j. Gu, M.z. Haq, M. Lawes, and R. Woolley. Original Articles: Laminar burning velocity and Markstein lengths of methane–air mixtures. *Combustion and Flame*, 121:41–58, 2000/1/1/2000///.

[22] Christine M. Vagelopoulos and Fokion N. Egolfopoulos. Direct experimental determination of laminar flame speeds. *Symposium (International) on Combustion*, 27:513–519, 1998/1/1/1998///.

[23] John B. Heywood. *Internal combustion engine fundamentals.* McGraw-Hill series in mechanical engineering. New York : McGraw-Hill, c1988., 1988.

[24] K.j. Bosschaart, L.p.h. de Goey, and in collaboration with J.M. Burgers Center for Fluid Mechanics. The laminar burning velocity of flames propagating in mixtures of hydrocarbons and air measured with the heat flux method. *Combustion & Flame*, 136(3):261, February 2004.

[25] Maogang He, Ying Guo, Qiu Zhong, and Ying Zhang. Determination of Binary Gas Diffusion Coefficients Using Digital Holographic Interferometry. *Journal of Chemical & Engineering Data*, 55(9):3318–3321, September 2010.